Iceberg discharges of the last glacial period driven by oceanic circulation changes

Jorge Alvarez-Solas[a,b,1], Alexander Robinson[a,b], Marisa Montoya[a,b], and Catherine Ritz[c]

[a]Universidad Complutense de Madrid, 28040 Madrid, Spain; [b]Instituto de Geociencias, Consejo Superior de Investigaciones Científicas–Universidad Complutense de Madrid, 28040 Madrid, Spain; and [c]Laboratoire de Glaciologie et de Géophysique de l'Environnement, Centre National de la Recherche Scientifique, 38402 Saint Martin d'Hères, France

Edited by Mark A. Cane, Lamont Doherty Earth Observatory of Columbia University, Palisades, NY, and approved August 22, 2013 (received for review April 12, 2013)

Proxy data reveal the existence of episodes of increased deposition of ice-rafted detritus in the North Atlantic Ocean during the last glacial period interpreted as massive iceberg discharges from the Laurentide Ice Sheet. Although these have long been attributed to self-sustained ice sheet oscillations, growing evidence of the crucial role that the ocean plays both for past and future behavior of the cryosphere suggests a climatic control of these ice surges. Here, we present simulations of the last glacial period carried out with a hybrid ice sheet–ice shelf model forced by an oceanic warming index derived from proxy data that accounts for the impact of past ocean circulation changes on ocean temperatures. The model generates a time series of iceberg discharge that closely agrees with ice-rafted debris records over the past 80 ka, indicating that oceanic circulation variations were responsible for the enigmatic ice purges of the last ice age.

glacial climate variability | climate modeling | abrupt changes

Compared with the present interglacial period, the last glacial period (LGP) (~110–10 ka before the present), and almost certainly previous ones (1), were characterized by substantial climatic variability on millennial timescales. This variability is mainly manifested in two types of events. Dansgaard–Oeschger (D/O) events are most notable in Greenland ice core records and involve decadal-scale warming of more than 10 K (interstadials) followed by slow cooling lasting several centuries and a final more rapid fall to cold background (stadial) conditions (2). Heinrich (H) events consist of massive iceberg discharges from the Laurentide Ice Sheet at intervals of ~7 ka during peak glacial conditions throughout the LGP (3). Both D/O and H events are associated with widespread centennial- to millennial-scale climatic changes, including a synchronous temperature response over the North Atlantic and an antiphase temperature relationship over Antarctica and most of the Southern Ocean, as revealed by a wealth of deep-sea sediments, ice core, and terrestrial records (4). The Atlantic meridional overturning circulation (AMOC) is thought to play a central role in these abrupt glacial climatic changes. Although the paleoceanographic evidence on this link is scarce and mostly restricted to a few high-resolution deep-sea sediment records of the last deglaciation (5, 6), both modeling studies and reconstructions provide strong support for the hypothesis that D/O events were caused by reorganizations of the AMOC (7, 8). H events, identified as enhanced ice-rafted detritus (IRD) in North Atlantic deep-sea sediments (3, 9), occur during climatic minima of the Northern Hemisphere. They have classically been attributed to internal oscillations of the Laurentide (10) and assumed to lead to important disruptions of the Atlantic Ocean circulation (11). However, paleoclimate data have revealed that most H events likely occurred about a thousand years after North Atlantic Deep Water (NADW) formation had already slowed down or largely collapsed (12, 13), implying that the initial AMOC reduction could not have been caused by the H events themselves. This evidence directly conflicts with the common interpretation that freshwater fluxes representing the iceberg discharges caused the shift into cold (i.e., stadial) conditions. This furthermore highlights the need for a new paradigm through which to understand the triggering mechanism of H events. As already advanced one decade ago (14), any new theory should be able to account for the fact that the cold periods in which H events appear are not caused by the iceberg discharges and that the latter occur systematically several centuries after the North Atlantic cooling. More recently, the interaction between ocean circulation and ice sheet dynamics has been suggested to play a major role in triggering H events (15–17). This hypothesis has been assessed in particular for the first H event, H1, with both models and data showing that reduced NADW formation and a weakened AMOC lead to subsurface warming in the Nordic and Labrador Seas. This results in rapid melting of the Labrador ice shelves causing substantial ice stream acceleration and enhanced iceberg discharge (18–20).

Here, we investigate the effects of oceanic circulation changes associated with millennial-scale climate variability on the Laurentide Ice Sheet dynamics within a more realistic modeling framework. To this end, we drive a hybrid ice sheet–ice shelf model (21) with time-varying oceanic subsurface temperature fields for the LGP (*Materials and Methods*) obtained by combining glacial climate simulations and information from proxy data. Climatic boundary conditions are otherwise fixed to glacial conditions, so that the only external forcing felt by the ice sheet model is the change in subsurface ocean temperatures. These are translated into basal melting rates via a linear equation dependent on a single tunable parameter (see *SI Text* for details and sensitivity tests). Climate simulations are performed with

Significance

Periodic episodes of massive iceberg discharges from the large Northern Hemispheric ice sheets into the North Atlantic Ocean occurred throughout the last glacial cycle. It is still not clear whether they resulted from internal ice dynamics alone or were possibly externally driven. Results of our simulations of the Laurentide Ice Sheet forced by oceanic circulation changes support the hypothesis that these ice discharges were induced by the collapse of a buttressing ice shelf and the subsequent acceleration of inland ice streams. This provides a new basis for understanding the dynamics of the coupled cryosphere–climate system of glacial cycles. Additionally, it has strong implications for the stability of the marine parts of the Antarctic ice sheet given anthropogenic oceanic warming.

Author contributions: J.A.-S., A.R., and M.M. conceived the initial idea; J.A.-S., A.R., and M.M. designed research; J.A.-S., A.R., and M.M. performed research; C.R. developed the ice sheet model; J.A.-S., A.R., and M.M. analyzed data; and J.A.-S., A.R., and M.M. wrote the paper.

The authors declare no conflict of interest.

This article is a PNAS Direct Submission.

[1]To whom correspondence should be addressed. E-mail: jorge.alvarez.solas@fis.ucm.es.

This article contains supporting information online at www.pnas.org/lookup/suppl/doi:10.1073/pnas.1306622110/-/DCSupplemental.

a global atmosphere–ocean model for glacial stadial and interstadial states (with weak and strong AMOC states, respectively) (22). These provide the range and spatial distribution of oceanic temperatures felt by the ice sheet. The temporal millennial-scale variability is based on a proxy-derived index used to interpolate in time between the stadial and interstadial ocean temperature fields. To produce this index, we assume that millennial-scale variability registered in the Greenland Ice Core Project (GRIP) δ^{18}O ice core record (2) reflects variations in the North Atlantic oceanic state (Fig. 1*A*). To characterize the latter, following previous work (1), we use a threshold in the derivative of the δ^{18}O GRIP signal to determine the timing of stadial to interstadial transitions (Fig. 1*B*). This allows for an objective classification of climatic states into stadials or interstadials (i.e., cold and warm surface periods). We furthermore assume millennial-scale variability as registered in the GRIP record reflects variations in NADW formation that have an imprint on subsurface temperatures in antiphase with respect to the surface state. Stadials are thus associated with periods of reduced NADW formation and weakened AMOC and warm subsurface temperatures, whereas during interstadials a stronger AMOC with active NADW formation cools the subsurface, in agreement with previous studies (15, 16, 19, 20, 23, 24). Considering a fast relaxation time of the subsurface temperature when convection resumes, and slow relaxation when convection is weak (20), we generate a subsurface warming index that slowly peaks during stadial climatic periods and more abruptly collapses when entering interstadial climatic periods (Fig. 1*C*). This index is thus directly derived from the GRIP time series and represents the only external forcing to the ice sheet model (see *Materials and Methods* and *SI Text* for details).

The application of subsurface oceanic forcing to the ice sheet model induces significant millennial-scale variability in the otherwise stable Laurentide Ice Sheet, as reflected in the velocity at the Hudson Strait outlet and iceberg discharge into the ocean (Fig. 2). For almost every peak in subsurface warming, there is a corresponding large and abrupt acceleration of the ice flow. Transitions between slow and fast states of the Hudson Strait ice stream occur several times during the LGP, with velocities varying between ~1,000 m·a^{-1} during buttressing periods and ~4,000 m·a^{-1} during periods of ice shelf breakup. The magnitude of the velocity does not directly correlate with the magnitude and duration of the subsurface warming, however, because of the competing timescales of ice sheet growth, ice advection from inland, and ice shelf breakup and growth. These three mechanisms lead to a nonlinear response of the system that appears to modulate the dynamics of the floating and inland ice in this region. When interstadial subsurface (i.e., cold) oceanic conditions are applied, the Labrador Sea ice shelf experiences low melt rates and can extend far enough to reach the western coast of Greenland (Fig. 3). In this way, significant backforce is felt by the Hudson Strait ice stream and velocities are greatly reduced. This allows the main Laurentide ice dome to grow and subsequently advect ice from inland toward the margin because of a permanently active Hudson Strait ice stream, preconditioning the ice sheet for more ice discharge into the ocean. When stadial subsurface (i.e., warm) oceanic conditions are applied, the ice shelf melts away from Greenland and no longer buttresses the ice stream that feeds it (Fig. 3). This allows a surge of velocity at the mouth of the ice stream, which propagates inland over several centuries and results in a significant increase in ice discharge into the Labrador Sea (Fig. 4). The magnitude of such a discharge event depends on the state of the ice sheet before the ice shelf collapse.

The simulated time series of calving into the Labrador Sea compares very well with proxies of calving obtained from marine

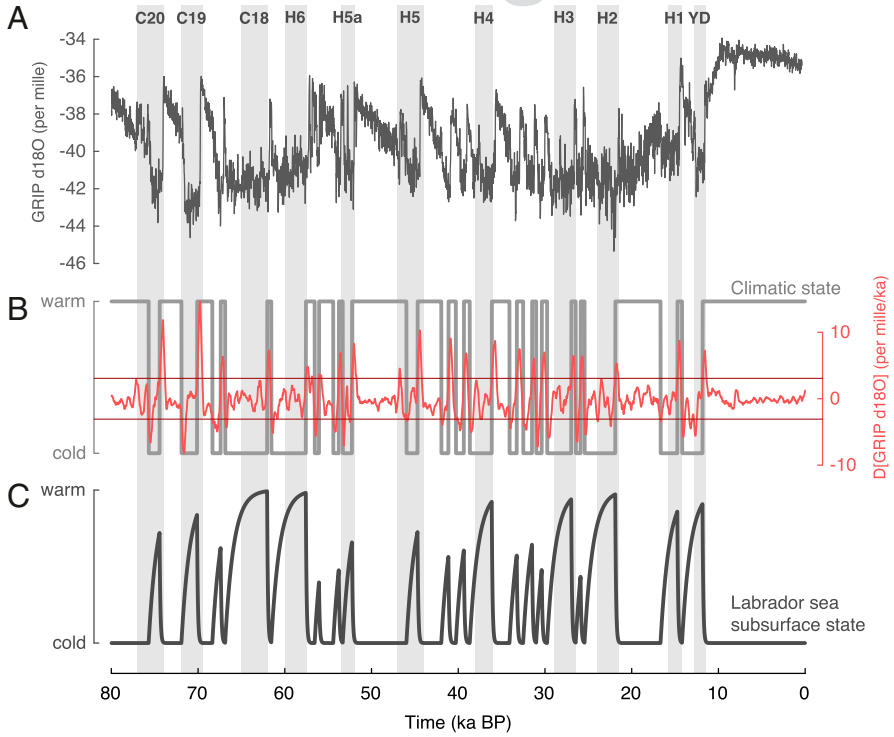

Fig. 1. Derivation of the Labrador Sea subsurface oceanic index. (*A*) GRIP d18O ice core record. (*B*) Smooth derivative of GRIP d18O record (red) with positive and negative thresholds which define transitions between stadial and interstadial states (grey). (*C*) Subsurface warming index. The cold subsurface state corresponds to an interstadial state (i.e., warm surface "climatic" state) with a mean subsurface (700- to 1,100-m depth) temperature of −0.9 °C. The warm subsurface state corresponds to a stadial state (i.e., cold surface "climatic" state) with a mean subsurface temperature of 1.1 °C.

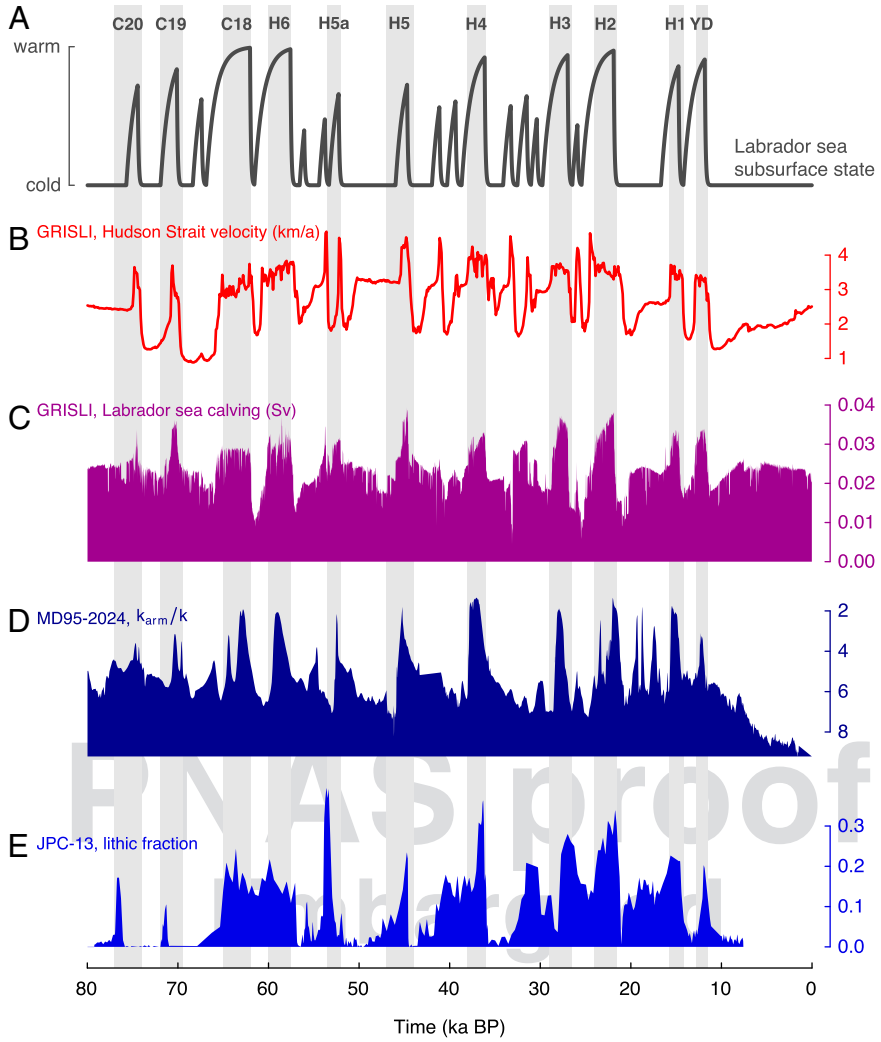

Fig. 2. (*A*) Labrador Sea subsurface oceanic index; (*B*) simulated Hudson Strait ice velocity (in kilometers per year); (*C*) simulated Labrador Sea calving rate (in Sverdrups); (*D*) magnetic susceptibility from core MD95-2024 (45.7°W, 50.2°N) (25); (*E*) lithic fraction from core JPC-13 (33.5°W, 53.1°N) (26). For the comparison, the timescales of the proxy data were converted to the SS09 timescale of the GRIP record (2).

sediment cores from the North Atlantic (Figs. 2 and 3). Both a high-resolution record of magnetic susceptibility from core MD95-2024 (45.7°W, 50.2°N) (25) and a record of lithic fraction from core JPC-13 (33.5°W, 53.1°N) (26), i.e., IRD proxies, show the same timing of peaks corresponding to major discharge events. In some isolated cases, such as between H4 and H3, or between H2 and H1, the simulated time series agrees better with the latter core. However, no spurious discharge events are simulated that are not apparent in at least one core. A comparison of the time series of the prescribed subsurface warming, calving, and IRD proxies highlights the fact that, for every strong peak in calving (i.e., H event), there is a necessary peak in subsurface warming. Several sensitivity tests with Grenoble ice shelf and land ice model (GRISLI) show that the amount of calving produced is a result of the nonlinear preconditioning of the ice sheet (*SI Text*). However, in our simulations the triggering mechanism for large ice discharges is always an ice shelf breakup precipitated by subsurface warming in the Labrador Sea. The strongest calving events are furthermore found to take place during the longest subsurface warming periods. We would expect the same relationship if subsurface temperature reconstructions were available, reflecting positive feedbacks operating between NADW formation and ice discharge (16). A more persistent reduction in NADW formation results in longer periods of subsurface warming. This in turn has a larger impact on ice shelves, which tends to increase ice discharge and suppress NADW formation further.

H events are among the most dramatic examples of millennial-scale variability of the Quaternary climate and their interpretation has remained elusive for decades. In recent years, the increasing availability of observations of the present-day ice sheets has confirmed the unexpected and crucial role that the ocean exerts on the dynamics of the ice sheets (27). Ice shelves represent the necessary interface for this coupled system. Whereas little information exists for a constrained reconstruction of the floating parts of the Laurentide, the maximum extent of the ice shelf simulated here is restricted to the continental shelf area between Greenland and the Hudson Strait. Such a configuration does not appear to contradict the relatively sparse proxy data available in this region (28), and is glaciologically consistent. Furthermore, the existence of a persistent ice stream through the Hudson Strait, as simulated here, is supported by geological evidence and modeling (29, 30).

Combined with the simulations presented here, the fact that the subsurface warming index generated from GRIP $\delta^{18}O$ data aligns so well with the IRD proxies lends strong support to the

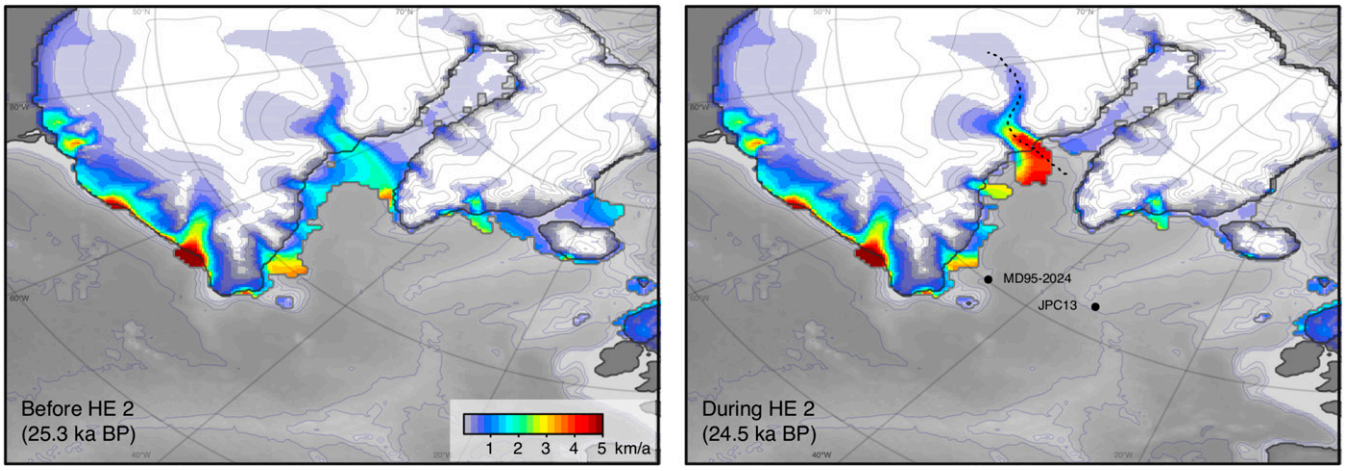

Fig. 3. Laurentide ice stream velocities (in kilometers per year) before (*Left*) and during (*Right*) H event 2, along with locations of the cores of the IRD proxies shown in Fig. 2. The dashed line in the right panel indicates the location of the profiles shown in Fig. 4.

hypothesis that millennial-scale glacial ice discharges are the result of a response to oceanic forcing. A characteristic time longer than the forcing timescale is the result of the nonlinearities of the ice sheet/ice shelf system. These arise from the different characteristic times of the ice shelf breakup and regrowth and by the time needed by the ice sheet to propagate the signal from its oceanic perturbation across the ice streams (Fig. 4). These phenomena favor the occurrence of resonance in the system and finally determine the observed pacing of ~7 ka.

Our simulations provide a physically based framework through which to understand the coupled ice sheet–ocean system. Open questions remain concerning the relationship between IRD proxies and actual calving rates, which can result from outburst floods, iceberg melting, and ocean circulation changes (31). One important related aspect concerns the fact that it is very difficult to constrain the melting rates that icebergs experience during their trip across the North Atlantic. This allows for alternative explanations considering the observed IRD belt as mainly the reflection of colder oceanic temperatures when Heinrich layers were formed (32). Under this interpretation, however, the amount of IRDs in marine cores close to the ice sheet source would reflect a signal absent of Heinrich-like events. This seems not to be the case, because Heinrich peaks can be observed in cores of the Labrador Sea (33). However, the explanation for the ultimate causes behind the underlying glacial oceanic variability remains elusive. Nonetheless, the work presented here shows that proxies and modeling reveal a consistent picture of the origin of the massive iceberg discharges of the last glacial cycle, including the enigmatic H events.

Materials and Methods

The ice sheet model GRISLI simulates the 3D evolution of the Laurentide using a hybrid ice sheet/ice shelf approach. GRISLI is one of the few models able to properly deal with both grounded and floating ice on the paleo-hemispheric scale, because it explicitly calculates grounding line migration, ice stream velocities, and ice shelf behavior. Inland ice deforms according to the stress balance using the shallow ice approximation (34, 35). Ice shelves are described following ref. 36, and ice streams (areas of fast flow, typically larger than $\sim 10^2$ m·y^{-1}) are considered as dragging ice shelves, allowing basal movement of the ice (37). Basal drag under ice streams is proportional to ice velocity and to the effective pressure. The locations of the ice streams are determined by the basal water within areas where the sediment layer is saturated. Contrary to the classic "binge–purge" theory (10), basal ice movement is computed here under the shallow shelf approximation. Rapid ice flow areas are therefore simulated in a more realistic dynamical approach (37). As a consequence, internal basal temperature oscillations, and thereby Laurentide instabilities, are found to vanish. In the absence of any oceanic forcing, the Laurentide Ice Sheet reaches a nonoscillatory steady state. Climate simulations are performed with CLIMBER-3α, which includes an oceanic general circulation model.

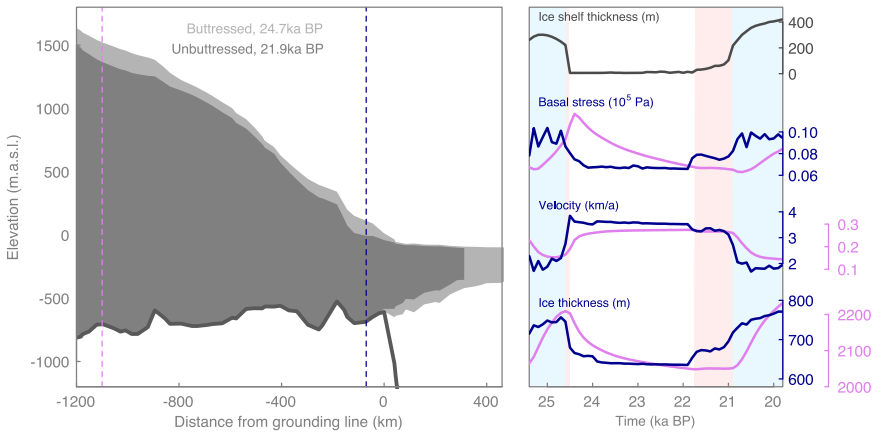

Fig. 4. Ice sheet profiles of the Laurentide (as indicated in Fig. 3) before and during HE2. Time series show ice-shelf thickness (gray; in meters), basal stress (10^5 Pa), velocity (in kilometers per year), and thickness (in meters) for the upstream (magenta) and downstream (dark blue) sections of the Hudson Strait ice stream. The background shading in the right panel represents buttressed (light blue), transition (light red) and unbuttressed (white) periods.

Basal melting rates under the ice shelves are computed here using a linear relationship on the difference between the subsurface temperature, T_o, and the temperature of the freezing point of salty waters, T_f:

$$B = \kappa(T_o - T_f), \quad [1]$$

where B is the basal melt rate under the Labrador Sea floating ice (in meters per year). T_o is the subsurface temperature of the Labrador Sea and its evolution through time is given by the following:

$$T_o \equiv T_o(t) = T_{is} + \alpha(t) \cdot (T_s - T_{is}). \quad [2]$$

Then,

$$\begin{array}{ll} \min(T_o) = T_{is}, & \text{when} \quad \alpha = 0 \\ \max(T_o) = T_s, & \text{when} \quad \alpha = 1, \end{array}$$

where $\alpha(t)$ is the subsurface warming index shown in Fig. 1, and T_s and T_{is} are the mean Labrador Sea subsurface temperatures for a stadial and an interstadial period, respectively.

The time series of IRD content from proxy data were converted to a common timescale with the model forcing for more direct comparison of the results. Namely, we used the original SS09 timescale (38) of the GRIP dataset (39) for all time series. The IRD record of ref. 25 was originally provided on the GISP2 timescale (40). Conveniently, the GRIP dataset included equivalent times between the SS09 and GISP2 timescales, allowing direct conversion of this time series to the SS09 timescale via linear interpolation. The IRD record of ref. 26 was provided on the SFCP timescale (41). Here, the equivalent times were only available for the newer SS09sea (42) timescale. In this case, we compared GRIP δ^{18}O values available on the SFCP timescale with the original data on the SS09 timescale, and optimized for the time corrections at 14 tie points (with linear interpolation in between) that would make the former match the latter. This procedure is accurate enough to allow for visual comparison on millennial timescales. For example, it is able to reproduce the SS09 δ^{18}O values with a root mean square error of 0.1 per mille. In Dataset S1, we provide equivalent times for the four timescales available (SS09, GISP2, SFCP, and SS09sea) for the last 80 ka.

ACKNOWLEDGMENTS. We thank A. Ganopolski for helpful discussions. This work was funded by the Spanish Ministry of Science and Innovation under the CGL08-06558-C02-01 project. The research leading to these results has also received funding from the European Union's Seventh Framework Programme (FP7/2007-2013) under Grant 243908, "Past4Future. Climate change - Learning from the past climate". A.R. is supported by the Marie Curie 7th Framework Programme.

1. Barker S, et al. (2011) 800,000 years of abrupt climate variability. *Science* 334:347–351.
2. Dansgaard W, et al. (1993) Evidence for general instability of past climate from a 250-kyr ice-core record. *Nature* 364:218–220.
3. Hemming SR (2004) Heinrich events: Massive Late Pleistocene detritus layers of the North Atlantic and their global climate imprint. *Rev Geophys* 42:RG1005.
4. Voelker A; Workshop Participants (2002) Global distribution of centennial-scale records for marine isotope stage (MIS) 3: A database. *Quat Sci Rev* 21:1185–1212.
5. McManus JF, Francois R, Gherardi JM, Keigwin LD, Brown-Leger S (2004) Collapse and rapid resumption of Atlantic meridional circulation linked to deglacial climate changes. *Nature* 428(6985):834–837.
6. Waelbroeck C, et al. (2011) The timing of deglacial circulation changes in the Atlantic. *Paleoceanography* 26:PA3213.
7. Broecker W (2006) Abrupt climate change revisited. *Global Planet Change* 54: 211–215.
8. Alley RB (2007) Wally was right: Predictive ability of the North Atlantic "conveyor belt" hypothesis for abrupt climate change. *Annu Rev Earth Planet Sci* 35:241–272.
9. Heinrich H (1988) Origin and consequences of cyclic ice rafting in the northeast Atlantic Ocean during the past 130,000 years. *Quat Res* 29:142–152.
10. MacAyeal D (1993) Binge/purge oscillations of the Laurentide Ice Sheet as a cause of the North Atlantic's Heinrich events. *Paleoceanography* 8:775–784.
11. Alley RB, Clark PU, Huybrechts P, Joughin I (1999) The deglaciation of the Northern Hemisphere: A global perspective. *Annu Rev Earth Planet Sci* 27:149–182, 10.1146/annurev.earth.27.1.149.
12. Hall IR, et al. (2006) Accelerated drawdown of meridional overturning in the late-glacial Atlantic triggered by transient pre-H event freshwater perturbation. *Geophys Res Lett* 33:L16616.
13. Jonkers L, et al. (2010) A reconstruction of sea surface warming in the northern North Atlantic during MIS 3 ice-rafting events. *Quat Sci Rev* 29:1791–1800.
14. Ganopolski A, Rahmstorf S (2001) Rapid changes of glacial climate simulated in a coupled climate model. *Nature* 409(6817):153–158.
15. Shaffer G, Olsen S, Bjerrum C (2004) Ocean subsurface warming as a mechanism for coupling Dansgaard-Oeschger climate cycles and ice-rafting events. *Geophys Res Lett* 31:L24202.
16. Flückiger J, Knutti R, White J (2006) Oceanic processes as potential trigger and amplifying mechanisms for Heinrich events. *Paleoceanography* 21:PA2014.
17. Alvarez-Solas J, et al. (2010) Links between ocean temperature and iceberg discharge during Heinrich events. *Nat Geosci* 3:122–126.
18. Hulbe C, MacAyeal D, Denton G, Kleman J, Lowell T (2004) Catastrophic ice shelf breakup as the source of Heinrich event icebergs. *Paleoceanography* 19:PA1004.
19. Alvarez-Solas J, et al. (2011) Heinrich event 1: An example of dynamical ice-sheet reaction to oceanic changes. *Clim Past* 7:1297–1306.
20. Marcott SA, et al. (2011) Ice-shelf collapse from subsurface warming as a trigger for Heinrich events. *Proc Natl Acad Sci USA* 108(33):13415–13419.
21. Ritz C, Rommelaere V, Dumas C (2001) Modeling the evolution of Antarctic ice sheet over the last 420,000 years: Implications for altitude changes in the Vostok region. *J Geophys Res* 106:31943–31964.
22. Montoya M, Levermann A (2008) Surface wind-stress threshold for glacial Atlantic overturning. *Geophys Res Lett* 35:L03608, 10.1029/2007GL032560.
23. Winton M, Sarachik E (1993) Thermohaline oscillations induced by strong steady salinity forcing of ocean general circulation models. *J Phys Oceanogr* 23:1389–1410.
24. Mignot J, Ganopolski A, Levermann A (2007) Atlantic subsurface temperatures: Response to a shut-down of the overturning circulation and consequences for its recovery. *J Clim* 20:4884–4898.
25. Stoner J, Channell J, Hillaire-Marcel C, Kissel C (2000) Geomagnetic paleointensity and environmental record from Labrador Sea core md95-2024: Global marine sediment and ice core chronostratigraphy for the last 110 kyr. *Earth Planet Sci Lett* 183:161–177.
26. Hodell D, Evans H, Channell J, Curtis J (2010) Phase relationships of North Atlantic ice-rafted debris and surface-deep climate proxies during the last glacial period. *Quat Sci Rev* 29:3875–3886.
27. Joughin I, Alley RB, Holland DM (2012) Ice-sheet response to oceanic forcing. *Science* 338(6111):1172–1176.
28. de Vernal A, Hillaire-Marcel C, Turon J, Matthiessen J (2000) Reconstruction of sea-surface temperature, salinity, and sea-ice cover in the northern North Atlantic during the last glacial maximum based on dinocyst assemblages. *Can J Earth Sci* 37:725–750.
29. Winsborrow M, Clark C, Stokes C (2004) Ice streams of the Laurentide Ice Sheet. *Geogr Phys Quatern* 58:269.
30. Stokes C, Tarasov L, Dyke A (2012) Dynamics of the North American ice sheet complex during its inception and build-up to the last glacial maximum. *Quat Sci Rev* 50:86–104.
31. Andrews J, et al. (2000) Icebergs and iceberg rafted detritus (ird) in the North Atlantic: Facts and assumptions. *Oceanography (Wash D C)* 13:100–108.
32. Kaspi Y, Sayag R, Tziperman E (2004) A triple sea-ice state mechanism for the abrupt warming and synchronous ice sheet collapses during Heinrich events. *Paleoceanography* 19:PA3004.
33. Rasmussen TL, Oppo DW, Thomsen E, Lehman SJ (2003) Deep sea records from the southeast Labrador Sea: Ocean circulation changes and ice-rafting events during the last 160,000 years. *Paleoceanography* 18:1018.
34. Morland L (1984) Thermomechanical balances of ice sheet flows. *Geophys Astrophys Fluid Dyn* 29:237–266.
35. Hutter K (1983) *Theoretical Glaciology: Material Science of Ice and the Mechanics of Glaciers and Ice Sheets* (Springer, Dordrecht, The Netherlands).
36. MacAyeal D (1989) Large-scale ice flow over a viscous basal sediment—Theory and application to ice stream B, Antarctica. *J Geophys Res* 94:4071–4087.
37. Bueler E, Brown J (2009) Shallow shelf approximation as a sliding lawin a thermomechanically coupled ice sheet model. *J Geophys Res* 114:F03008.
38. Johnsen SJ, Dahl-Jensen D, Dansgaard W, Gundestrup N (1995) Greenland palaeotemperatures derived from GRIP bore hole temperature and ice core isotope profiles. *Tellus B Chem Phys Meterol* 47:624–629.
39. Greenland Ice-Core Project Members (1993) Climate instability during the last interglacial period recorded in the grip ice core. *Nature* 364:203–207.
40. Sowers T, et al. (1993) A 135,000-year Vostok-specmap common temporal framework. *Paleoceanography* 8:737–766.
41. Shackleton N, Fairbanks R, Chiu T-c, Parrenin F (2004) Absolute calibration of the Greenland time scale: Implications for Antarctic time scales and for Δ^{14}C. *Quat Sci Rev* 23:1513–1522.
42. Johnsen SJ, et al. (2001) Oxygen isotope and palaeotemperature records from six Greenland ice-core stations: Camp century, dye-3, grip, gisp2, renland and northgrip. *J Quat Sci* 16:299–307.

Supporting Information

Alvarez-Solas et al. 10.1073/pnas.1306622110

SI Text

Models

The Ice Sheet Model. The model used in this study is the Grenoble ice shelf and land ice model (GRISLI) ice sheet–ice shelf model developed by Ritz et al. (1). It is a hybrid 3D thermomechanical ice sheet model combining shallow-ice and shallow-shelf approximations (SIA and SSA), able to deal both with grounded and floating ice on paleo and hemispheric scales, because it explicitly calculates the Laurentide grounding line migration, ice stream velocities, and ice shelf behavior.

The model has been used in several studies for simulating the evolution of Antarctica (1–3), Fennoscandia (4), the Laurentide Ice Sheet (LIS) (5, 6), and Greenland (7). A comprehensive description is given by these authors.

Ice Sheet Buildup and Climate Forcing. The climate forcing used to initially build the ice sheet is based on the surface climate fields simulated by the model CLIMBER3-α (8). Two snapshots of glacial and present climate simulations are used to provide surface air temperature (SAT) and precipitation values at each grid point through a glacial index method, where the maximum value corresponds to the Last Glacial Maximum (LGM). In this way, surface climate fields provided to the ice sheet model correspond to the present-day climatology corrected by the anomalies between the simulated climate of the LGM and that of the present-day interglacial. The atmospheric temperature also includes a lapse rate adjustment dependent on the elevation of the ice sheet surface. This method has been used in many studies to simulate the evolution of the cryosphere during the last glacial cycle (e.g., ref. 9). This procedure was found by Alvarez-Solas et al. (5) to lead to Northern Hemisphere ice sheet characteristics at the LGM showing good agreement with reconstructions in terms of volume, geographical distribution, and ice stream locations (10, 11). For the purpose of this paper, a time-invariant surface climate forcing corresponding to permanent glacial conditions is imposed. A constant external forcing is also used in similar studies devoted to the study of the Laurentide ice discharges (12, 13). Two main improvements with respect to previous simulations of the millennial dynamics of the LIS are derived from the use of a hybrid approach. First, it allows consideration of the evolution of the floating parts of the ice sheet. At the same time, ice streams are now treated under the SSA, and therefore there is no need to impose any amplification factor on basal sliding to reasonably reproduce the fast flow areas of the ice sheet (5, 6, 14–16). In this way, a control simulation, considering constant basal melting rates under the ice shelves, shows a stable behavior of the LIS with no distinguishable ice purges or internal oscillations. This differs from previous studies based on ice sheet models based on the SIA only, where a thermomechanical feedback was shown to create oscillations when basal sliding was amplified enough (12, 13). The disappearance of this oscillatory behavior here is due to a better representation of the heat flux created by basal dragging that favors a stabilization of the ice streams dynamics. In this case, the steady-state ice stream velocity mainly depends on the amount of backforce exerted by an ice shelf at its mouth.

The Subsurface Warming Mechanism

The heating of high-latitude subsurface waters as a consequence of the shift between interstadial and a stadial period is a combination of advective and diffusive processes. The ultimate cause of such a warming is related to the enhanced stratification inhibiting vertical mixing in the Nordic Seas that allows the intermediate layers to warm, but as described by Mignot et al. (17) using the same model as ours, the suppression of this intermediate ventilation allows the penetration of relatively warm water coming from the south to high northern latitudes beneath the halocline, in the Nordic Seas. The anomaly is subsequently transported into the Labrador Sea through the subpolar gyre on advective timescales.

The first study, to our knowledge, describing this mechanism was one using a simplified, diffusive model (18) that led to slow warming of the whole Atlantic basin above 2,500-m depth after an Atlantic meridional overturning circulation (AMOC) shutdown through downward diffusion. However, the subsurface warming has subsequently been confirmed through a different, nondiffusive mechanism (5, 17) and by others, such as the ECBILT-CLIO model (19) or the CCSM3 model (20). One important difference between the study of Mignot et al. (17) and ours is that their simulations were carried out in a present-day background climate framework. The authors mentioned in their conclusions that it would be necessary to assess its validity in a glacial climate context, which we now confirm.

However, a number of marine sediment cores have shown that cold stadial conditions are associated with subsurface and intermediate depth warming in the North Atlantic (21–23), thus lending strong support to the model results.

On the Subsurface Warming Index

As mentioned in the main text, the surface climate was chosen to be time-invariant to better discriminate the effects of the imposed oceanic forcing on Laurentide variability. Hence, subsurface ocean temperature variations are considered to calculate basal melting rates under the floating part of the Laurentide. To this end, following a similar approach to that shown by Barker et al. (24), we consider the derivative of the GRIP $\delta^{18}O$ curve (25) with respect to time and define two states (stadial and interstadial) and two thresholds (high and low; Fig. 1). The system remains in a given state as long as the threshold leading to the other state is not surpassed. We further assume millennial-scale climate variability (basically, Dansgaard–Oeschger events) are caused by variations in North Atlantic Deep Water (NADW) formation. In other words, we make the assumption that millennial variability registered in Greenland is mainly the expression of the North Atlantic oceanic state. This, in turn, has an effect on subsurface temperatures. Stadials are associated with periods of reduced NADW formation and warm subsurface temperatures, whereas during interstadials, active NADW formation cools the subsurface, in agreement with previous studies (5, 17–19, 22). Subsurface warming following from the reduction in NADW formation is slow compared with more rapid cooling of the subsurface (17). This is implemented by relaxing subsurface temperatures within each state to predefined stadial and interstadial subsurface temperature reference levels, with a longer relaxation time for the stadial than for the interstadial (1 and 0.1 ky, respectively). The resulting ocean subsurface temperature time series is then imposed on the model, while the surface climate (SATs, precipitation) is kept constant at its glacial state. The proposed subsurface oceanic index (i.e., the idea that subsurface temperatures exhibit two main states and relax to a given one in antiphase with respect to temperatures registered in Greenland) is consistent with recent simulations of stadial–interstadial transitions with the CLIMBER3-α model (17, 26)

and with several new proxy interpretations (22, 23, 27, 28). Therefore, during warm surface periods (i.e., interstadials) NADW formation is strong, sea surface temperatures are relatively high and the polar front extended further north. Deep-water formation in the Labrador Sea during this period favors the mixing of the subsurface waters by convection; thus, relatively cold waters are simulated in CLIMBER3-α. The Labrador Sea mean subsurface temperature is $T_{is} = -0.86$ °C. During cold surface periods (i.e., stadials), the AMOC shows a weakened state, the polar front expands southward, and convection in the Labrador Sea is strongly reduced. This results in a halocline, the isolation of subsurface waters that warm up to 3 °C in some places, with a mean subsurface warming of 1.95 °C. In this case, the Labrador Sea mean subsurface temperature is now $T_s = 1.09$ °C. All time series displayed in the main text correspond to the experiment carried out with $\kappa = 0.4$ m·a^{-1}·K^{-1}. This translates into mean basal melt rates of $B_{is} = 0.376$ m·a^{-1} and $B_s = 1.156$ m·a^{-1}. Observed basal melting rates under the Antarctic ice shelves are extremely variable in space, and although the latter numbers fall in the range of observed Antarctic values (29), we decided to test the validity of our main results to different values of κ. The following sections analyze the Laurentide iceberg discharges for several sensitivity experiments.

Oceanic Temperature and Ice Shelf Basal Melt: Dependence on κ

Figs. S1 and S2 show the model response in terms of calving and ice velocities for different values of κ. Thirteen values of κ were considered, ranging from 0.05 to 1.5 m·a^{-1}·K^{-1}.

For the lowest value of this parameter ($\kappa = 0.05$ m·a^{-1}·K^{-1}), subsurface warming is not capable of producing breakup of the Labrador ice shelves, and therefore the velocities of the Hudson Strait ice stream at the grounding line remain constant at a value of ~2.2 km·a^{-1}. Thus, no significant calving peaks are simulated during the recorded periods of enhanced IRDs deposition (highlighted in gray in Fig. S1). Only when κ is increased to a value of 0.15 m·a^{-1}·K^{-1} do ice shelves break up for some of the periods of warmer subsurface waters, ice velocities start to be modulated at the millennial scale, and iceberg discharges begin to be distinguishable during the periods of high IRDs . For κ values between 0.2 and 0.9 m·a^{-1}·K^{-1}, ice velocities and calving curves are highly similar to the ones shown in the main text (i.e., the standard simulation corresponding to $\kappa = 0.4$ m·a^{-1}·K^{-1}).

When κ is increased to 1.0 m·a^{-1}·K^{-1}, the backforce exerted by the ice shelves during periods of cold subsurface waters, and thus during rebuttressing periods, decreases. Ice shelves become thinner and less extended, implying less efficient buttressing; however, calving peaks are still simulated at the right periods. In this case, the associated acceleration of the Hudson Strait ice stream is less evident, so ice velocities do not significantly drop during cold subsurface periods and millennial-scale iceberg discharges begin to diminish.

This effect becomes stronger for higher values of κ and reaches a threshold for $\kappa = 1.5$ m·a^{-1}·K^{-1}, above which ice shelves are unable to regrow during cold periods of the subsurface waters. This favors a permanent reduction of their backforce exerted on the Hudson Strait grounding line and allows steady-state ice velocities (up to ~ 3.8 km·a^{-1}) and stable low levels of calving.

The large range of κ values for which the millennial iceberg discharges can be reproduced with a remarkable agreement with IRD records gives further robustness to the mechanism proposed in the main text.

Laurentide Response to Idealized Oceanic Periodic Forcings

It has been shown in the main text that the shape of the calving curves obtained as a response to the oceanic index arises from the presence of nonlinearities inherent to the coupled dynamics of the floating and inland ice. The present section aims to illustrate the related processes by imposing simpler and fully periodic oceanic indices to the ice sheet model. Different periodic forcings have been considered, keeping the main shape of the transitions, which derives from two different relaxation times: 1 ka for warming and 0.1 ka for cooling. Several main periods of the forcing were taken into account between 1 and 10 ka. Fig. S3 shows three illustrative examples corresponding to periods of 2, 3, and 7 ka and for the standard κ value of 0.4 m·a^{-1}·K^{-1}. This latter value determines the magnitude of the oceanic subsurface warming a priori ensuring an ice shelf breakup and is therefore appropriate to investigate the inland response of the ice sheet and its impact on the iceberg discharges depending on different forcing periodicities.

The three calving curves of Fig. S3 show an essentially "one-to-one" response with respect to the applied oceanic forcing. However, the response is not simply linear, with some of the peaks showing an amplitude up to fivefold the amplitude of others. This response reflects to the preconditioning of the inland ice before the ice shelf breaks up. A thicker grounding line would cause a higher iceberg discharge for the same increase in velocities. Conversely, the grounding-line thickness depends on the buttressing that the ice shelf has been exerting, but also on the gravitational driving stress of the ice stream, which depends, in turn, on the elevation of the ice stream source. The inland propagation of the grounding line perturbations (caused by the ice shelf variability) is then a crucial process for determining the timing of iceberg discharges. The different characteristic times of the processes described here favor the occurrence of some resonance in the timing of the iceberg discharges (see spectra in Fig. S3).

The periodicity of the oceanic glacial variability typically ranges between 1.5 and 6 ka (30). Regarding our ice sheet results, the perturbation exerted by the ice shelf removal diffuses toward the ice stream source within ~100 a, whereas the kinematic wave does so within ~700 a. These processes are therefore relatively fast. However, once the oceanic perturbation is stopped, the time necessary to recover the former state can be as large as 10 ka, depending on the duration of the oceanic perturbation. This effect is investigated through additional sensitivity experiments in the following section.

Ice Flow Under Idealized "delta" Experiments

Four different step functions of the same amplitude but different length (0.15, 2, 5, and 10 ka) are applied as oceanic forcing (Fig. S4). A short oceanic warming of 150 y is enough to cause an ice shelf breakup, but regrowth is almost instantaneous, allowing a rebuttressing effect and a drop of the ice velocities that slowly (i.e., ~3 ka) tend to recover to the initial value. A similar result is reproduced for a subsurface warming duration of 2 ka, with sustained enhanced velocities during the perturbation. For the intermediate perturbation time of 5 ka, a highly nonlinear response appears in the ice flow. For the whole duration of the perturbation, ice velocities remain at high values of around 4 km·a^{-1}, which progressively thins the grounding line. By the time the oceanic perturbation is stopped, the ice shelf becomes larger, and when it touches the west coast of Greenland, the ice at the grounding line decelerates. This deceleration, together with a thinner grounding line, results in only weak ice flow toward the ice shelf that is not enough to maintain its extended length (even under cold subsurface temperatures). This translates into a secondary breakup and associated acceleration. Once again, the ice shelf tends to overextend and it is only when the grounding line has been fed enough because of enhanced gravitational stress that the ice flux toward the ice shelf helps to maintain a permanent buttressing ice shelf. A similar process is simulated for the longest forcing (10 ka), with the difference that enhanced velocities during a longer period make the rebuilding of the ice shelf longer and not subject to the previous "rebound" effect.

The different characteristic times of ice shelf breakup and regrowth, together with the distinct responses of the inland-floating ice flow depending on the duration of the oceanic perturbation, further contribute to the nonlinearities described in the previous section.

The sensitivity tests shown here explain the nonlinear response of the iceberg discharges to the oceanic index described in the main text. As a summary, the amount of calved icebergs obviously depends on the amplitude and duration of the subsurface warming experienced by the ice shelves. However, ultimately, the calving will be strongly modulated by other associated processes. A thick grounding line at the Hudson Strait ice stream favors a great discharge. If the gravitational driving stress is initially high (determined by a steep slope between the mouth and the source of the ice stream), a given calving event will be sustainably amplified or not, depending on whether the ice shelf remains unbuttressed for a long or a short period. On the contrary, if gravitational stress is initially low, a given calving event will not be amplified by an "inland" effect if the subsurface warming is short, but will later be amplified if the breakup lasts long enough for the kinematic wave to propagate inland, favoring an enhancement of the ice flow toward the ocean.

1. Ritz C, Rommelaere V, Dumas C (2001) Modeling the evolution of Antarctic ice sheet over the last 420,000 years: Implications for altitude changes in the Vostok region. *J Geophys Res* 106:31943–31964.
2. Alvarez-Solas J, et al. (2001) Millennial-scale oscillations in the Southern Ocean in response to atmospheric CO_2 increase. *Global Planet Change* 76:128–136.
3. Philippon G, et al. (2006) Evolution of the Antarctic ice sheet throughout the last deglaciation: A study with a new coupled climate–North and South Hemisphere ice sheet model. *Earth Planet Sci Lett* 248:750–758.
4. Peyaud V, Ritz C, Krinner G (2007) Modelling the Early Weichselian Eurasian Ice Sheets: Role of ice shelves and influence of ice-dammed lakes. *Clim Past* 3:375–386.
5. Alvarez-Solas J, et al. (2011) Heinrich event 1: An example of dynamical ice-sheet reaction to oceanic changes. *Clim Past* 7:1297–1306.
6. Alvarez-Solas J, Robinson A, Ritz C (2012) Brief communication: Can recent ice discharges following the Larsen-B ice-shelf collapse be used to infer the driving mechanisms of millennial-scale variations of the Laurentide Ice Sheet? *The Cryosphere* 6:687–693.
7. Quiquet A, et al. (2012) Sensitivity of a Greenland ice sheet model to atmospheric forcing fields. *The Cryosphere* 6:999–1018.
8. Montoya M, et al. (2005) The Earth System Model of Intermediate Complexity CLIMBER-3α. Part I: Description and performance for present day conditions. *Clim Dyn* 25:237–263.
9. Charbit S, Ritz C, Philippon G, Peyaud V, Kageyama M (2007) Numerical reconstructions of the Northern Hemisphere ice sheets through the last glacial-interglacial cycle. *Clim Past* 3:15–37.
10. Winsborrow M, Clark C, Stokes C (2004) Ice streams of the Laurentide Ice Sheet. *Geogr Phys Quatern* 58:269–280.
11. Stokes C, Tarasov L (2010) Ice streaming in the Laurentide Ice Sheet: A first comparison between data-calibrated numerical model output and geological evidence. *Geophys Res Lett* 37:L01501.
12. Calov R, Ganopolski A, Petoukhov V, Claussen M, Greve R (2002) Large-scale instabilities of the Laurentide Ice Sheet simulated in a fully coupled climate-system model. *Geophys Res Lett* 29(24):2216.
13. Papa B, Mysak L, Wang Z (2006) Intermittent ice sheet discharge events in northeastern North America during the last glacial period. *Clim Dyn* 26:201–216.
14. Bueler E, Brown J (2009) Shallow shelf approximation as a sliding lawin a thermomechanically coupled ice sheet model. *J Geophys Res* 114:F03008.
15. Tarasov L, Dyke A, Neal R, Peltier W (2012) A data-calibrated distribution of deglacial chronologies for the North American ice complex from glaciological modeling. *Earth Planet Sci Lett* 315-316:30–40.
16. Stokes C, Tarasov L, Dyke A (2012) Dynamics of the North American ice sheet complex during its inception and build-up to the last glacial maximum. *Quat Sci Rev* 50:86–104.
17. Mignot J, Ganopolski A, Levermann A (2007) Atlantic subsurface temperatures: Response to a shut-down of the overturning circulation and consequences for its recovery. *J Clim* 20:4884–4898.
18. Shaffer G, Olsen S, Bjerrum C (2004) Ocean subsurface warming as a mechanism for coupling Dansgaard-Oeschger climate cycles and ice-rafting events. *Geophys Res Lett* 31:L24202.
19. Flückiger J, Knutti R, White J (2006) Oceanic processes as potential trigger and amplifying mechanisms for Heinrich events. *Paleoceanography* 21:PA2014.
20. Brady E, Otto-Bliesner B (2011) The role of meltwater-induced subsurface ocean warming in regulating the Atlantic meridional overturning in glacial climate simulations. *Clim Dyn* 37:1517–1532.
21. Rasmussen TL, Thomsen E (2004) The role of the North Atlantic drift in the millennial timescale glacial climate fluctuations. *Palaeogeogr Palaeoclimatol Palaeoecol* 210: 101–116.
22. Marcott SA, et al. (2011) Ice-shelf collapse from subsurface warming as a trigger for Heinrich events. *Proc Natl Acad Sci USA* 108(33):13415–13419.
23. Dokken TM, Nisancioglu KH, Li C, Battisti DS, Kissel C (2013) Dansgaard-Oeschger cycles: Interactions between ocean and sea ice intrinsic to the Nordic seas. *Paleoceanography*, in press.
24. Barker S, et al. (2011) 800,000 years of abrupt climate variability. *Science* 334:347–351.
25. Dansgaard W, et al. (1993) Evidence for general instability of past climate from a 250-kyr ice-core record. *Nature* 364:218–220.
26. Banderas R, Álvarez-Solas J, Montoya M (2012) Role of CO_2 and Southern Ocean winds in glacial abrupt climate change. *Clim Past* 8:1011–1021.
27. Gutjahr M, Hoogakker B, Frank M, McCave I (2010) Changes in North Atlantic deep water strength and bottom water masses during marine isotope stage 3 (45–35kabp). *Quat Sci Rev* 29:2451–2461.
28. Gutjahr M, Lippold J (2011) Early arrival of southern source water in the deep North Atlantic prior to Heinrich event 2. *Paleoceanography* 26:PA2101.
29. Jenkins A, Corr H, Nicholls K, Doake C, Stewart C (2003) Measuring the basal melt rate of Antarctic ice shelves using GPS and phase-sensitive radar observations. *FRISP Report* 14:1–8.
30. Ganopolski A, Rahmstorf S (2002) Abrupt glacial climate changes due to stochastic resonance. *Phys Rev Lett* 88(3):038501.

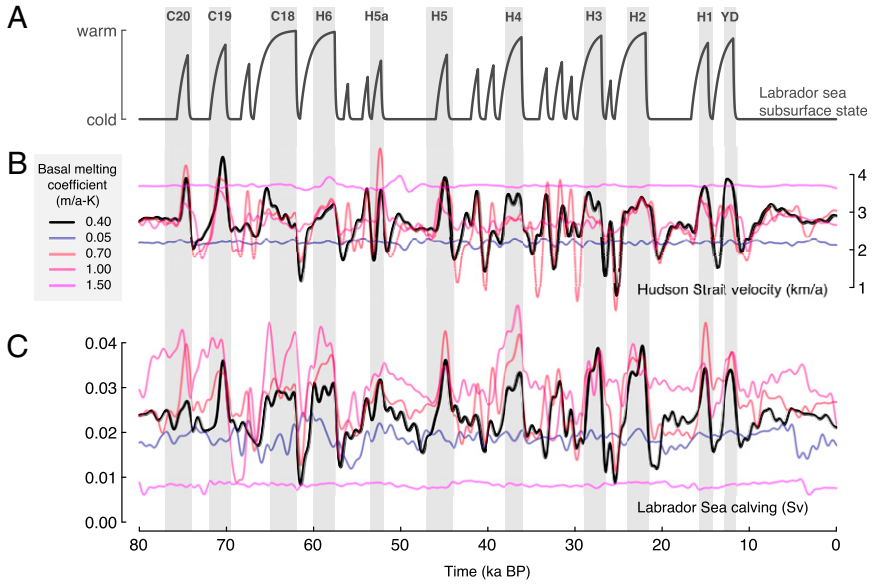

Fig. S1. Subsurface oceanic index (*A*). Ice velocities at the Hudson Strait grounding line (*B*), and calved icebergs to the Labrador Sea (*C*) for five different values of the parameter κ.

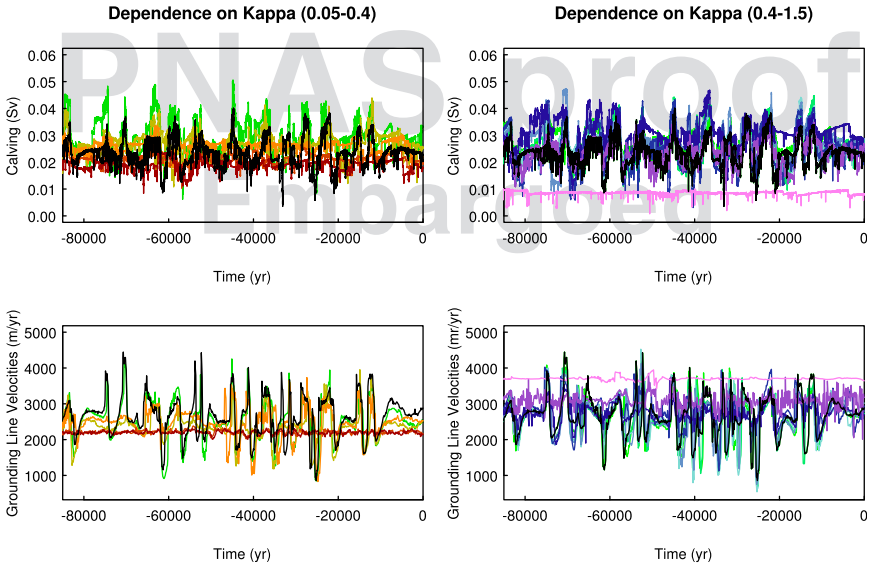

Fig. S2. Iceberg discharges (*Upper*) and Hudson Strait ice velocities (*Lower*) for different values of the κ parameter (ranging from 0.05 to 1.5 $m{\cdot}a^{-1}{\cdot}K^{-1}$) relating oceanic temperatures to basal melt under ice shelves.

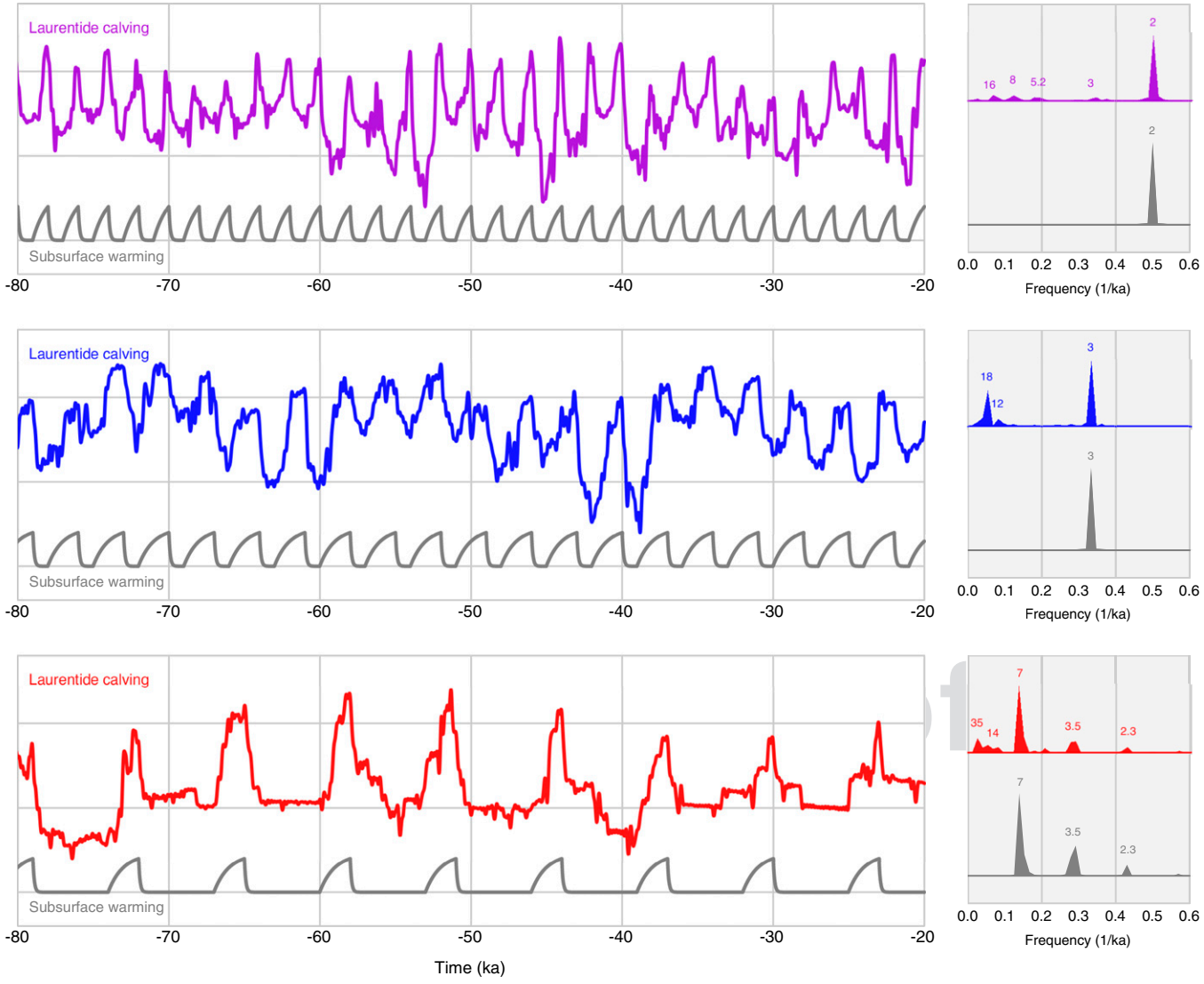

Fig. S3. Laurentide calving response (pink, blue, and red; from *Top* to *Bottom*) to idealized oceanic forcings of 2-, 3-, and 7-ka periodicities, respectively. The associated spectra are shown in the right part of each panel. The numbers labeling the peaks are in kiloyears.

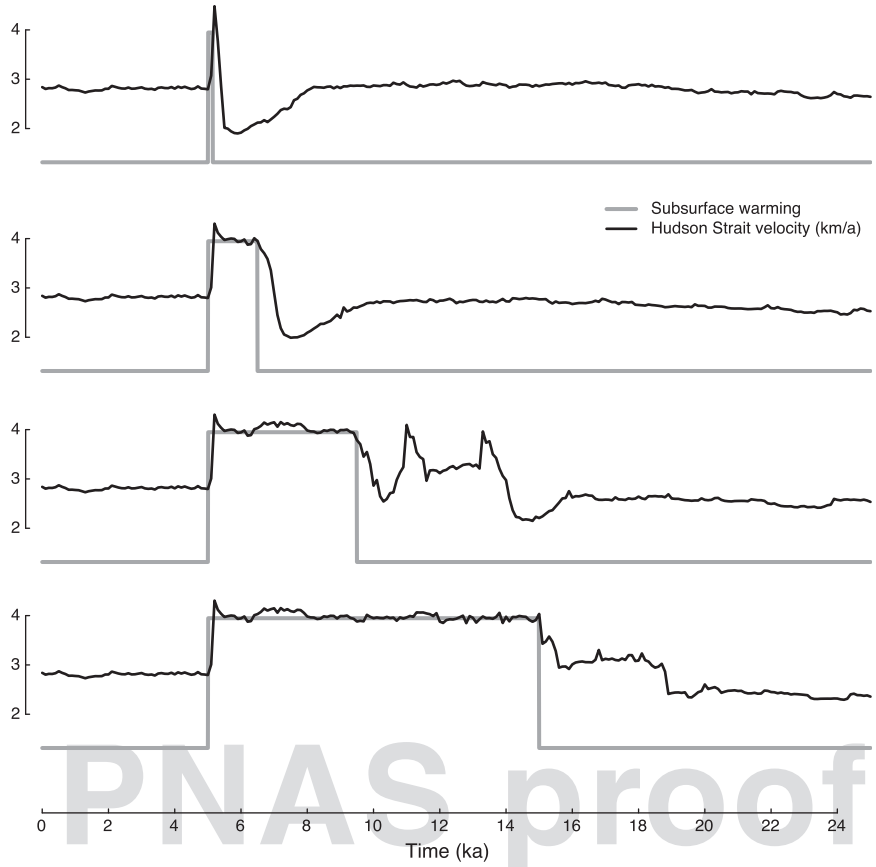

Fig. S4. Hudson Strait ice velocities at the grounding line for four different forcings based on step functions of lengths 0.15, 2, 5, and 10 ka (from *Top* to *Bottom*).

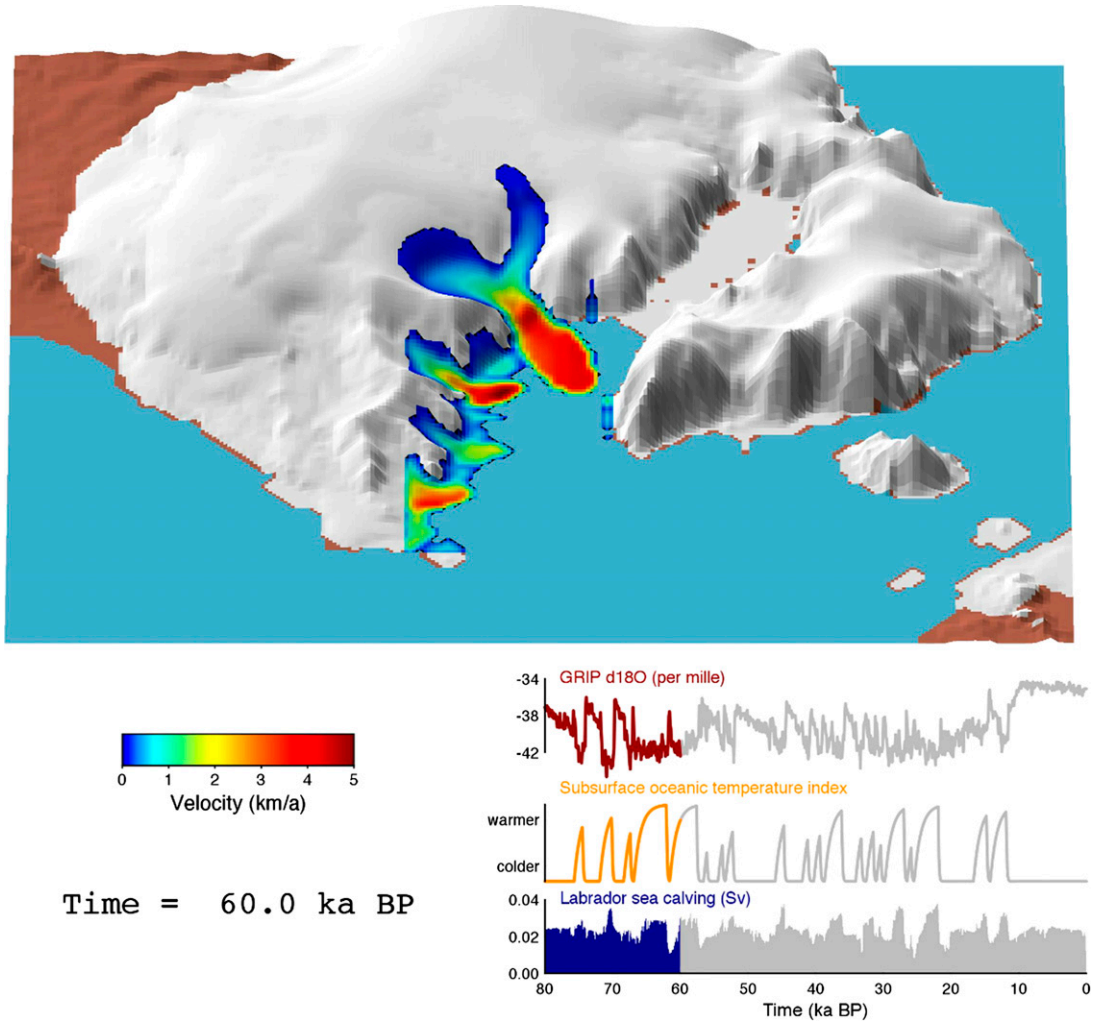

Movie S1. Animation of the Laurentide and Greenland ice sheets. Hudson Bay/Strait ice stream velocities are illustrated in colors. The time series at *Bottom* show the evolution of the GRIP d18O core, the subsurface oceanic index, and the simulated calving of icebergs into the Labrador Sea.

Movie S1

Other Supporting Information Files

Dataset S1 (TXT)